Proceedings of the Korean Nuclear Spring Meeting
Gyeong ju, Korea, May 2003

Countercurrent Flow Limited CHF in a 3 x 3 rod bundle with a non-uniform axial heat flux

Seok Cho, Se-Young Chun, Sang-Ki Moon, Won-Pil Baek

Korea Atomic Energy Research Institute
150 Deokjin-Dong, Yuseong-Gu, Daejeon, 305-353, Korea

Abstract

KAERI has performed an experimental study of water critical heat flux (CHF) under zero flow conditions with a non-uniformly heated 3 by 3 rod bundle. Experimental conditions are in the range of a system pressure from 0.5 to 15.0 MPa and inlet water subcooling enthalpies from 67.5 to 351.5 kJ/kg. The test section used in the present experiments consisted of a vertical flow channel, upper and lower plenums, and a non-uniformly heated 3 by 3 rod bundle. The experimental results show that the CHFs in low-pressure conditions are somewhat scattered within a narrow range. As the system pressure increases, however, the CHFs show a consistent parametric trend. The CHFs occur in the upper region of the heated section, but the vertical distances of the detected CHFs from the bottom of the heated section are reduced as the system pressure increases. Even though the effects of the inlet water subcooling enthalpies and system pressure in the flooding CHF are relatively smaller than those of the flow boiling CHF, the CHF increases by increasing the inlet water subcooling enthalpies. Several existing correlations for the countercurrent flooding CHF based on Wallis's flooding correlation and Kutateladze's criterion for the onset of flooding are compared with the CHF data obtained in the present experiments to examine the applicability of the correlations.

1. Introduction

Many investigators have carried out experimental and/or analytical studies on the countercurrent flow limited critical heat flux (CHF) under zero inlet flow or very low flow conditions for practical interests to predict the performance such as closed end thermosyphon reboilers and nuclear reactor core accident situations, including a flow transient in case of reactor coolant pump failure and flow stagnation and flow reversal characteristics of the loss-of-coolant accident (LOCA) (Barnard , 1974; Chang, 1991; Katto, 1991; Nejat, 1981; Tien, 1979). The reactor coolant flow is reduced during a large portion of several types of accident scenarios, and the core encounters the stagnant or reverse flow. In this condition, the vapor flows up from the heated section while the liquid falls down from the upper plenum due to gravity. When the heat input is sufficiently large, the vapor flow causes countercurrent-flow limitation (CCFL) or flooding at the top, which leads to a liquid deficiency in the heated section. Hence the CHF is limited by flooding, which we call flooding CHF. Therefore, the precise understanding of the fundamental nature of CHF in the vertical flow channel under the flooding conditions will be important for reactor safety, inasmuch as the flooding CHF results in the minimum value and limits a heat transfer rate much lower than the pool-boiling CHF.

The flooding CHF mechanism may be different from that of other kinds of CHF such as the pool or flow boiling CHF with respect to the fact that the fundamental mechanism of the flooding CHF is dominated by the flooding phenomenon at the top of the heated channel. In case of a vertical channel with a large liquid volume or short heated section, the CHF mechanism becomes similar to the departure from nucleate boiling (DNB) in pool boiling. However, the mechanism for a narrow and

long vertical channel under zero flow conditions may be different from that of the pool boiling CHF. The empirical flooding correlations have been useful to estimate the CHF in a heated vertical channel for zero flow or low flow conditions with the assumption of the mass and energy balance. One of the most frequently used correlations for flooding was given by Wallis (1969), in the following expression:

$$j_g^{*1/2} + m j_l^{*1/2} = C_w \tag{1}$$

where j_g^* and j_l^* are the dimensionless superficial velocities of vapor and liquid, respectively. C_w is a constant, mainly depending upon the channel end conditions. The constant m is set to unity for the turbulent flow. The dimensionless superficial velocities j_g^* and j_l^* are defined by

$$j_g^* = j_g \rho_g^{1/2} (gD\Delta\rho)^{-1/2} \tag{2}$$

$$j_l^* = j_l \rho_l^{1/2} (gD\Delta\rho)^{-1/2} \tag{3}$$

where j_g and j_l are the superficial velocities of gas and liquid, respectively, D is the inner diameter of the tube, and $\Delta\rho$ is the density difference between the liquid and vapor phases. Several investigators, however, have employed Kutateladze's criterion for the onset of flooding, given by the following equation:

$$K_g^{1/2} + m K_l^{1/2} = C_k \tag{4}$$

where K_g and K_l are defined by $K_g = j_g \rho_g^{1/2} (g\sigma\Delta\rho)^{-1/4}$ and $K_l = j_l \rho_l^{1/2} (g\sigma\Delta\rho)^{-1/4}$, respectively, and C_k is a constant. Pushkina and Sorokin gave m = 0, C_k = 3.2 for the flooding condition (Bankoff and Lee, 1983).

The previous studies on the flooding CHF might be categorized into two types according to the test geometry – that is to say a vertical channel with and without a liquid reservoir at the top of the heated channel. Chun et al. (2001) performed the experimental study for the zero-flow condition with a reservoir by using an annulus channel. From the comparison of the data with the existing flooding CHF correlations, he showed that the correlations depend greatly on the effect of the heat flux distribution of the heated section. Imura et al. (1983) made the CHF test for the closed-bottom vertical channels without a reservoir, and proposed an experimental correlation, which shows a +/-30% error band with their data. Mishima et al. (1987) maintained that the CHF due to flooding increases with an increasing diameter and decreasing heated length until it reaches the pool-boiling CHF. They also pointed out that different flow channel geometries could affect the flooding CHF phenomenon and proposed the constant C_w of Eq. (1) is 1.66, 0.98, and 0.73 for tubes, annuli, and rectangular channels, respectively.

The bulk of the previous studies in this area, however, have been performed by using annulus, rectangular ducts and a single round tube to investigate the fundamental mechanism of the flooding CHF. Until now, to the authors' knowledge, CHF experiments in a multi-rod bundle with a non-uniformly heated section under high-pressure conditions have not been carried out. Therefore, this paper presents the results of the flooding CHF experiments carried out with a non-uniformly heated 3 by 3 rod bundle and with the water reservoir under extended pressure conditions. Several existing correlations for the countercurrent flooding CHF are compared with the present CHF data to examine the applicability of the correlations.

2. Experimental Descriptions

2.1 Experimental Facility

The CHF experiments have been conducted in the Reactor Coolant System thermal hydraulics loop facility (RCS loop facility) of the Korea Atomic Energy Research Institute (KAERI). Detailed descriptions on the RCS facility can be found in Chun et al. (2000). The test section used in the present experimental work is described in this section.

Figure 1 shows the details of the test section used in the present experiments. The test section consists of a vertical 3 by 3 channel and upper and lower plenums. The upper plenum is connected to

a steam/water separator. The 3 by 3 rod bundle is located in a square shroud whose lateral dimension is 39.8mm. The mean outer diameter and heating length of a heater rod at room temperature is 9.52mm and 3,673mm, respectively. The pitch of the 3 by 3 rod array is 12.6mm as depicted in Fig. 1. The heater rods are heated indirectly by electricity. The sheath and heating element of the heater rods are made of Inconel 600 and Nichrome, respectively. Heater rods with non-uniform axial power distributions are used in the present work. For measuring the heater rod surface temperature and detecting the CHF occurrence, 6 elements of Chromel-Alumel thermocouple with a sheath outer diameter of 0.5mm are embedded on the outer surface of a heater rod. (The total number of embedded thermocouples of 9 heater rods is 44 elements) Figure 2 shows the axial power distribution of the heater rods. The power level is divided into 15 steps with a minimum and maximum power ratio of 0.440 and 1.369, respectively, to simulate a symmetric chopped cosine heat flux profile. The temperature sensing points on the heater rod surface are located at 10, 225, 625, 1025, 1425, and 1825mm from the top end of the heater rod.

The main parameters measured in the experiments are the water temperatures and pressures at the inlet and outlet plenums, and the 32 elements of subchannel temperatures at the bottom and top of the heater rod, the surface temperatures of the heater rod, the differential pressures in the test section, and the power applied to the test section. All the electrical signals from the sensors and transmitters are treated and analyzed by a data acquisition and control system consisting of the A/D and D/A converter and a workstation computer. The uncertainties of the measuring system were estimated from the calibration of sensors and the accuracy of the equipment, according to a propagation error analysis based on the Taylor series expansion (ANSI/ASME PTC 19.1, 1985). The evaluated maximum uncertainties of pressures and temperatures were less than +/-0.3% and +/-0.7% K of the readings in the range of interest, respectively. The uncertainties of the heat flux calculated from the applied power were always less than +/-1.8% of the readings.

2.2 Experimental Procedure and Conditions

The present experiments have been performed using the following procedure. At first, the circulation pump, preheater and pressurizer are operated for raising the temperature of the loop and establishing inlet subcooling and pressure of the test section at the desired levels, and the isolation valve located at the upstream of the test section is fully closed. Power is applied to the heater rod and increased gradually in small steps. The period between the power steps is chosen to be sufficiently long (about 10 minutes) so that the loop could stabilize in the steady-state conditions. As the power to the heater rod increases, the temperatures in the upper plenum and connecting pipe to the steam/water separator reach the saturated temperature. A countercurrent flow is then formed in the heated section. As the loop approaches a CHF condition, the temperature fluctuation at the surface of the heater rod is detected. The CHF condition in the present study is determined when the surface temperature of the heater rod continuously rises and then becomes 110 K higher than the saturated temperature. Whenever the CHF is detected, the heater power is automatically tripped to prevent any damage of the heater rod.

A total of 56 CHF data were obtained in the experimental ranges of the inlet water subcooling enthalpies from 67.5 to 351.5 kJ/kg at the bottom end of the heated section and system pressures from 0.5 to 15.0MPa. The pressure at the top end of the heated section is specified as the system pressure and is used for the analysis of the measured data.

3. Experimental Results and Discussions

3.1 Observation of CHF Behaviors

Since rapid power increase can cause an irregular event related to an imbalance between the fall of condensed water from the upper plenum and the rising of evaporated vapor in the heated section, the power input to the heater rod was carefully increased. If the rapid power increase or short period between the power steps was applied to the heater rod before the water temperature in the upper

plenum reached the saturation temperature, rapid temperature rise throughout the surface of the heater rod was frequently observed in low heat flux conditions. This phenomenon is due to the sudden evaporation of water in all regions of the heated surface area under unstable conditions, while the stable countercurrent flow does not form yet. This situation is not desired in the present work.

Figure 3 shows the typical local wall temperature variation of the heater rods at CHF conditions with time. When the power level reaches the CHF condition, the surface temperatures measured by T/C 3 and 4 embedded at 625 and 1025mm below from the top end of the heated section, respectively, rise almost linearly without fluctuations. The temperature of T/C 2 installed at the location of 225mm below, however, shows a nearly constant value at some degree of superheating, except that there are several fluctuations. The other surface temperatures of the heater rod such as T/C 1, 5, and 6 maintain a constant saturation value and the large temperature fluctuations are not observed during a run of the experiments. This type of temperature variation was observed in the entire pressure range of the present experiments. The surface temperature variation of the heater rods illustrated in Fig. 3 is similar to that observed in the study of Katto et al. (1991) conducted in uniformly heated tubes with a liquid reservoir at the top of the heated section. Chun et al. (2001) who performed the flooding CHF experiments in an annulus flow channel with uniformly and non-uniformly heated sections over a pressure range of 0.52 – 14.96 MPa also observed this type of temperature behavior only at high pressures of 12.08 and 14.96 MPa.

In the present experiments, the locations of the CHF occurrence can be divided into three groups in terms of system pressure. At low-pressure regions of 0.5 and 1.0 MPa, the CHF occurred mainly at the locations of 10 and 225 (T/C 1 and 2,), and sometimes 625mm (T/C 3) from the top end of the heated section. On the other hand, the CHF was detected only by the T/C 3 in the intermediate pressure ranges such as 3, 6, 9 MPa. Finally, at high-pressure conditions of 12.0 and 15.0 MPa, the CHF always occurred 1025mm from the top end of the heated section (T/C 4). Moreover, as the system pressure increased more than 6.0 MPa, the CHF always detected at the central heating rod (R5 in Fig. 1). The reasons why the location of the CHF occurrence moves in a downward direction and toward the central rod with the increase of the system pressure are not interpreted satisfactorily yet, but one of the reasons can be understood with respect to the upward velocity of the vapor and the geometry effect of the present test section. When the relative velocity between the upward-flow of vapor and downward-flow of liquid reaches a critical value, a flooding phenomenon occurs and the falling liquid film in the heater rod array reaches a stagnant condition (Wallis, 1969). If the relative velocity exceeds this critical value, the liquid is then taken in the upward direction somewhere of the test section by the upward-flow of the vapor. Since an amount of water is supplied continuously from the upper plenum, the location of the minimum liquid film thickness pushes in a upward direction as the upward velocity of the vapor increases. Hwang et al. (1994) predicted the CHF locations for a boiling tube with a closed bottom on the basis of the assumption that dryout occurs at the boundary between the two-phase mixture and the countercurrent annular flow regions owing to the evaporation of the falling film. The density ratio of liquid to vapor and the latent heat of vaporization at the saturated condition become small as the system pressure increases. The liquid to vapor density ratio, however, shows a stronger reduction trend than the latent heat of vaporization with the increase of the pressure. An amount of steam generated in the test section at the saturated state is proportional to the applied electrical power and inversely proportional to the latent heat of vaporization. The trend of the applied electrical power with the variation of the pressure and the inlet water subcooling enthalpy at the CHF condition can be seen in Fig. 4, which shows that the electrical power increases up to a pressure of 3 MPa and decreases as the pressure is further increased. With the results shown in Fig. 4 and the relationship between the steam generation rate and the latent heat of vaporization with respect to the pressure, it can be roughly estimated that the amount of steam produced in the test section does not show a great difference with the increase of the pressure. Therefore, the velocity of steam in the 3 by 3 rod array is slowed down as the pressure increases due to the effect of steam density.

3.2 Data Reduction

In the present study, the data reduction methodology proposed by Chun et al. (2001) has been adopted to analyze the experimental data and is presented briefly in this section. Since the water at the bottom part of the heated section is under a subcooled condition at the instant of a CHF, the amount of steam generated in the heated section cannot be evaluated directly from the mass and energy balances. In order to determine the locations of the onset of saturated boiling in their experiments, Chun et al. (2001) assumed that the pressure losses due to the friction and acceleration can be neglected for the gravitational pressure loss, ΔP, between the bottom end of the heated section (Z = 0) and a location Z and the void fraction in the subcooled boiling region is negligibly small. Considering physical model depicted in Fig. 5. The ΔP is equal to the static heat from the bottom end of the heated section to the location Z. Consequently, the average void fraction, α, from the bottom end (Z = 0) to the location Z is given by

$$\alpha = \frac{\rho_{l,sat} g Z + (\rho_{l,sub} - \rho_{l,sat}) g Z_{sat} - \Delta P}{(\rho_{l,sat} - \rho_g) g (Z - Z_{sat})} \tag{5}$$

where ρ_l and ρ_g are the liquid and vapor densities, and g is the gravitational acceleration. The subscripts 'sub' and 'sat' denote the subcooled and saturation conditions, respectively.

In the present study, the pressure difference, ΔP, is set to the sum of the value measured by DP-03, 04, and 05 in Fig. 1. The trends of ΔP as a function of subcooling temperature, ΔT_{sub}, at the bottom end of the heated section are given in Fig. 6, which shows the linear relationship between ΔP and ΔT_{sub} for a fixed system pressure except for 0.5 and 1 MPa. The pressure difference for ΔT_{sub} = 0 (i.e. Z_{sat} = 0) can be calculated from the extrapolation of the linear relationship of the two parameters. Substituting the value of ΔP, Z (in the present study, Z = 1,101 m) and Z_{sat} = 0 into Eq. (5), the average void fraction, α_0, for the saturated condition at the bottom end of the heated section is calculated for each system pressure. When it is assumed that α decreases linearly in proportion to the increase in distance Z_{sat}, the void fraction α is expressed as follows:

$$\alpha = \alpha_0 \left(1 - \frac{Z_{sat}}{Z} \right) \tag{6}$$

The location of the onset of saturated boiling can be calculated from Eq. (5) and (6) and the pressure difference. Subsequently, the boiling length, L_B, at CHF condition is defined by the heated length, L_h, as follows:

$$L_B = L_h - Z_{sat} \tag{7}$$

The average CHF, $q_{C,B}$, over the boiling length is expressed by

$$q_{C,B} = \frac{1}{L_B} \int_{Z_{sat}}^{L_h} q(z) dz \tag{8}$$

where $q(z)$ is the axial heat flux profile of the heater rod. The $q_{C,B}$ calculated from Eq. (8) are presented in Fig. 7 as a function of the boiling length to the heated equivalent diameter ratio, L_B/D_{he}, calculated by using Eq. (7). The CHFs decrease with L_B/D_{he} although the values are somewhat scattered due to the effect of pressure. Katto et al. (1992) indicated that the magnitude of the CHF is approximately inversely proportional to the heated length of the tube at a fixed condition of tube diameter.

3.3 Existing Correlations for the Flooding Limited CHF

Up to the present, the Wallis's flooding correlation, Eq. (1), and Kutateladze's criterion, Eq. (4), for the onset of flooding have been widely applied to estimate the CHF for zero flow or very low flow conditions with the assumption of mass and energy balance. For the boiling system shown in Fig. 5, when the heated area, A_B, over the boiling length is employed, the following mass and energy balance equation holds under steady-state conditions:

$$j_g \rho_g A_f = j_l \rho_l A_f = \frac{q_{C,B} A_B}{h_{lg}} \tag{9}$$

where A_f is the flow area of the channel, and h_{lg} is the latent heat of vaporization. Substituting Eq. (9) into Eq. (1) and using a hydraulic equivalent diameter, D_{hy}, in Eqs. (2) and (3) for the present channel, the CHF due to flooding is expressed in a dimensionless form as the following equation:

$$\frac{q_{C,B}}{h_{lg}(gD_{hy}\rho_g\Delta\rho)^{1/2}} = \frac{C_w}{4}\left(\frac{D_{he}}{L_B}\right)\left[1+\left(\frac{\rho_g}{\rho_l}\right)^{1/4}\right]^{-2} \tag{10}$$

In the above equation, the heated equivalent diameter to the boiling length ratio, $D_{he}/(4L_B)$, was used instead of the term A_f/A_B. The CHF, $q_{C,B}$, and the boiling length, L_B, are calculated from Eqs. (8) and (7), respectively.

Mishima et al. (1987) rewrote Eq. (10) as follows:

$$\frac{q_{C,B}}{h_{lg}(g\lambda\rho_g\Delta\rho)^{1/2}} = \frac{C_w^{\,2}}{4}\left(\frac{D_{he}}{L_B}\right)D^{*1/2}\left[1+\left(\frac{\rho_g}{\rho_l}\right)^{1/4}\right]^{-2} \tag{11}$$

where D^* is the dimensionless diameter, defined by $D^*=D_{hy}/\lambda$. The length scale, λ, of the Taylor instability is given by $\lambda = (\sigma/g\Delta\rho)$, where σ is the surface tension. Therefore, D^* used by Mishima is equal to the Bond number, $B_o = D_{hy}(g\Delta\rho/\sigma)^{1/2}$. They reported that their flooding CHF Data are well correlated by Eq. (11) with C_w = 0.98 for an annulus. Nejat (1981) proposed a flooding CHF correlation based on Eq. (10). Nejat added the correction term $(L_B/D)^{-0.1}$ in the correlation in order to reduce the scatter of the experimental data points on the tubes. Using the CHF $q_{C,B}$ in the heated surface and the heated equivalent diameter, Nejat's correlation can be rewritten as

$$\frac{q_{C,B}}{h_{lg}\rho_g(gD_{hy})^{1/2}} = \frac{C_w^{\,2}}{4}\left(\frac{D_{he}}{L_B}\right)\left(\frac{\Delta\rho}{\rho_g}\right)^{1/2}\left[1+\left(\frac{\rho_g}{\rho_l}\right)^{1/4}\right]^{-2} \tag{12}$$

where $C_w^{\,2}$ is $0.36(L_B/D_{he})^{0.1}$.

Tien et al. (1979) proposed a flooding CHF correlation based on Kutateladze's criterion, Eq. (4), given by the following expression:

$$\frac{q_{C,B}}{h_{lg}(g\sigma\rho_g^{\,2}\Delta\rho)^{1/4}} = \frac{C_k^{\,2}}{4}\left(\frac{D_{he}}{L_B}\right)\left[1+\left(\frac{\rho_g}{\rho_l}\right)^{1/4}\right]^{-2} \tag{13}$$

where $C_k^{\,2}$ = $3.2[\tanh(B_o^{1/4}/2)]^2$. The term on the left-hand side of Eq. (13) is sometimes called the Kutateladze number employed in many CHF correlations for pool boiling. The empirical correlation with a similar form to Eq. (13) was derived by Imura et al. (1983). The correlation is expressed by

$$\frac{q_{C,B}}{h_{lg}(g\sigma\rho_g^{\,2}\Delta\rho)^{1/4}} = \frac{C_k^{\,2}}{4}\left(\frac{D_{he}}{L_B}\right)\left(\frac{\rho_g}{\rho_l}\right)^{-0.13} \tag{14}$$

Imura et al. reported that Eq. (15) with $C_k^{\,2}$ = 0.64 correlated the experimental data within +/-30 % accuracy.

Mishima et al. (1987) reported that the flooding CHF is correlated using Eq. (11) with C_w = 1.66, 0.98 and 0.73 for tubes, annuli and rectangular channels, respectively. In Nejat's Eq. (11), C_w was modified with the term of L_B/D, and Tien et al. (1979) proposed Eq. (14) with a correction term relating to the Bond number B_o for C_k. This implies that the values of C_w and C_k are not constant and vary with the geometry and thermodynamic conditions. Park et al. (1997) examined the effects of the terms L_B/D_{he}, Bo, and ρ_g/ρ_l on $C_w^{\,2}$ using Eq. (10) and proposed the empirical correlation for $C_w^{\,2}$ with a RMS (root mean square) error of 18.8%.

$$C_w^{\,2} = 1.22\left(\frac{L_B}{D_{he}}\right)^{0.12}\left(\frac{\rho_g}{\rho_l}\right)^{0.064}(1+0.055B_o-4.08\times10^{-3}B_o^{\,2}) \tag{15}$$

Chun et al. (2001) indicated that the range of the density ratio used in the development of C_w^2 of Park et al. does not cover their experimental conditions and also proposed the empirical correlation for C_w^2 to enhance the coherence of the experimental data within a RMS error of 9.0%.

$$C_w^{\,2} = 1.22\left(\frac{L_B}{D_{he}}\right)^{0.12}\left(\frac{\rho_g}{\rho_l}\right)^{-0.032}(1+0.055B_o-4.08\times10^{-3}B_o^{\,2}) \quad (16)$$

Table 1 shows the present test conditions and applicable ranges of the correlations of Park et al. (1997) and Chun et al. (2001).

3.4 Comparison with the Existing Correlations

Katto et al. (1991) pointed out that the right-hand side of Eq. (13) is nearly equivalent to the right-hand side of Eq. (10) except for the value of C_w^2. Chun et al. (2001) indicated that the use of the Bond number term, $\tanh(B_o^{1/4}/2)$, of Tien et al. (1979) produces a large difference between their experimental data and the calculated values and the form of the Bond number term of Tien, et al. may not be appropriate. Actually, Katto et al. (1992) and Park et al. (1997) discussed and examined the applicability of Eq. (13) with $\tanh(B_o^{1/4}/2) = 1$, and used $C_k^2 = 3.2$, to correlate their CHF data. The correlations of Park et al. and Chun et al., Eq. (15) and (16), respectively, were derived on the basis of the Wallis flooding equation. Therefore, in the present study, the values of $3.2C_w^2$ and C_w^2 calculated from Eqs. (15), and (16) are used as C_k^2 of the correlations of Tien et al., Eq. (13), and Imura et al., Eq. (14), respectively.

As mentioned above, the Kutateladze number is employed in the left-hand side of Eqs. (13) and (14), and the left-hand side of Eq. (11) proposed by Mishima et al. (1987) is also equal to the Kutateladze number. To compare the present data with Eqs. (10), (11), (12), (13), and (14), the dimensionless parameters are defined as follows:

$$q^*_{C,w} = \frac{q_{C,B}}{h_{lg}(gD_{hy}\rho_g\Delta\rho)^{1/2}},\quad q^*_{C,N} = \frac{q_{C,B}}{h_{lg}\rho_g(gD_{hy})^{1/2}},$$

$$q^*_{C,k} = \frac{q_{C,B}}{h_{lg}(g\sigma\rho_g^2\Delta\rho)^{1/4}},\ \text{and}\ \xi = \left[1+\left(\frac{\rho_g}{\rho_l}\right)^{1/4}\right]^{-2}$$

Figures 8 ~ 12 show the results of the comparison between the present data and the existing correlations. As can be seen in Figs. (8), (9), (11), and (12), the present data show a large scattering, especially in the high-pressure region, and have noticeable differences with the existing correlations. In Fig. 8, 9, and 10 for the Wallis-type correlations, even though the dimensionless parameters, q^*_C, calculated from Eq. (10), (11), and (12) show considerably underestimated values than the present data when the values of C^*_w suggested by the original investigators are used, q^*_C calculated by using C^*_w suggested by Park et al. (1997) give somewhat enhanced trends toward the present data. Especially, at the pressure condition of 6 MPa, the present data show a good agreement with the correlated values. In the higher- and lower-pressure condition, however, the correlated values are gradually diverging from the present values. When C^*_w proposed by Chun et al. (2001) is applied in Eq. (10), (11), and (12), the dimensionless parameters, q^*_C, show little more difference than when C^*_w by Park et al. is applied to the corresponding equations.

The comparisons of the present data with the Kutateladze-type correlations such as Eqs. (13) and (14) are made in Figs. (11) and (12), which show the present data lie between the two correlated lines of Park et al. (1997) and the original investigators such as Tien et al. (1979) and Imura et al. (1983). A large scattering can be observed at high-pressure regimes of 9, 12, and 15 MPa, and the degree of scattering becomes large as the system pressure increases. At the low-pressure regions of 3 and 6 MPa, however, the scattering of the present data is reduced considerably, and the experimental data show a linear trend. When the values of $3.2C^*_w$ and C^*_w calculated by Eq. (16) are used as C^*_k in Figs. (11) and (12), respectively, the magnitude of the dimensionless parameter, q^*_C, shows remarkably

overestimated values than those of the present data, but the overall trend of these two data sets is very similar – i.e. the angle of a slope is nearly the same.

3. Conclusions

The counetercurrent flow limited critical heat flux experiments have been carried out to investigate the characteristics of a flooding CHF in a non-uniformly heated 3 x 3 rod bundle over a wide pressure range of 0.5 - 15.0 MPa. The present data are compared with several existing flooding CHF correlations such as those proposed by Mishima et al. (1987), Nejat (1981), Tien and Chung (1979), Imura et al. (1983), Park et al. (1997), and Chun et al. (2001). The present study leads to the following conclusions.

(1) When the power level reaches the CHF condition, the surface temperatures near the CHF location rise almost linearly without fluctuations to the preset value of CHF detection. In the CHF condition, temperatures at the lower part of the heated section maintain a constant saturation value and the large temperature fluctuations are not observed. This type of temperature variation was observed in the entire pressure range of the present experiments.
(2) The CHFs occur in the upper region of the heated section, but the location of the CHF occurrence moves in a downward direction and toward the central rod with the increase of system pressure. This is mainly due to the geometry effect of the present test section.
(3) The CHFs decrease with the ratio of the boiling length to the heated equivalent diameter, L_B/D_{he}, although the values are somewhat scattered due to the effect of pressure.
(4) For the Wallis-type correlations, q^*_C calculated by using the correlation of Park et al. for C^*_w show a reasonable agreement with the present data, especially, at the pressure condition of 6 MPa. In the higher- and lower-pressure condition, however, the correlated values are gradually diverging from the present values.
(5) The comparisons with the Kutateladze-type correlations show the present data lie between the two correlated lines of Park et al. (1997) and the original investigators. Although scattering of the present data in the high-pressure regimes is large, it is reduced considerably in the low-pressure region.
(6) When the value of C^*_w calculated by Eq. (16) are used as C^*_k in the Kutateladze-type correlations, the magnitude of q^*_C shows remarkably overestimated values than those of the present data, but the overall trend of these two data sets is very similar.

Nomenclature

A_B	heated area of the boiling length, m^2
A_f	cross sectional flow area of a channel, m^2
C_k	constant in the Kutateladze flooding criterion
C_w	constant in the Wallis flooding equation
D_{he}	heated equivalent diameter, m
D_{hy}	hydraulic equivalent diameter, m
D^*	dimensionless diameter, D_{hy}/λ
g	gravitational acceleration, m/s^2
h_{lg}	latent heat of evaporation, kJ/kg
h_{sub}	subcooling enthalpy at the bottom end of the heated section, K
j	superficial velocity, m/s
j^*	dimensionless superficial velocity, $j\rho^{1/2}(gD\,\Delta\rho)^{-1/2}$
K	Kutateladze number, $j\rho^{1/2}(g\sigma\,\Delta\rho)^{-1/4}$
L_B	boiling length in the heated section, m
L_h	heated length, m
P	pressure, MPa
P	differential pressure, kPa

Q_T total applied electrical power at the instant of CHF condition, kW
$q(z)$ axial heat flux profile of the heater rod, kW/m^2
$q_{C,B}$ average critical heat flux over the boiling length, kW/m^2
$q^*_{C,k}$ dimensionless CHF parameter in Eqs. (11), (13) and (14) , $q_{C,B}/[h_{lg}(g\sigma\rho_g{}^2\Delta\rho)^{1/4}]$
$q^*_{C,N}$ dimensionless CHF parameter in Eq. (12), $q_{C,B}/[h_{lg}\rho_g(gD_{hy})^{1/2}]$
$q^*_{C,w}$ dimensionless CHF parameter in Eq. (10), $q_{C,B}/[h_{lg}(gD_{hy}\rho_g\Delta\rho)^{1/2}]$
T_{sub} subcooling temperature at the bottom end of the heated section, K
Z distance from the bottom end of the heated section, m

Greek symbols

α average void fraction from the bottom end of the heated section to location Z
λ length scale of Taylor instability, $(\sigma/g\Delta\rho)^{1/2}$, m
ρ density, kg/m^3
$\Delta\rho$ density difference of liquid and vapor phase, $\rho_l - \rho_g$, kg/m^3
σ surface tension, N/m
ξ dimensionless parameter in the flooding CHF equations, $[1+(\rho_g/\rho_l)^{1/4}]^{-2}$

Subscripts

C critical heat flux
B boiling length
g vapor phase
k Kutateladze's flooding criterion
l liquid phase
N Nejat's correlation
sat saturation condition
sub subcooled condition
w Wallis's flooding equation

Acknowledgement

This research has been performed as a part of the long-term nuclear energy development program supported by the Ministry of Science and Technology (MOST) of Korea.

References

1. ANSI/ASME PTC 19.1, 1985, ASME Performance Test Codes, Supplement on Instruments and Apparatus, Part 1, Measurement Uncertainty, ASME, New York.
2. Bankoff, S. G., Lee, S. C., 1983, A critical review of the flooding literature, NUREG/CR-3060 R2, Northwest University, USNRC, pp.70-71.
3. Barnard, D. A., Barnard, D. A., Stinchcombe, R. A., 1974, Dryout at low mass velocities for an upward boiling flow of refrigerant-113 in a vertical tube, UKEA, AERE-R 7726.
4. Chang, S. H., Baek, W. P., Bae, T. M., 1991, A study of critical heat flux for low flow of water in vertical round tube under low pressure, *Nucl. Eng. Des.,* **132**, pp.225-237.
5. K. Mishima, H. Nishihara, 1987, Effect of channel geometry on critical heat flux for low pressure water, *Int. J. Heat Mass Transfer*, **30(6)**, pp.1169-1182.
6. Z. Nejat, 1981, Effect of density ratio on critical heat flux in closed end vertical tube, *Int. J. Multiphase Flow,* **7**, pp.321-327.
7. Chun, S. Y., et al., 2000, Critical heat flux in uniformly heated vertical annulus under a wide range of pressure – 0.57 to 15.0 MPa, *J. Korean Nucl. Soc.*, **32**, pp.128-141

8. Chun, S. Y., et al., 2001, Critical heat flux under zero flow conditions in vertical annulus with uniformly and non-uniformly heated sections, *Nuclear Engineering and Design*, **205**, pp.265-279.
9. C. Park, et al., 1997, Countercurrent flooding limited critical heat flux in vertical channels at zero inlet flow, *Int. Comm. Heat Mass Transfer*, **24(4)**, pp.453-464.
10. H. Imura, et al., 1983, Critical heat flux in a closed two-phase thermosyphon, *Int. J. Heat Mass Transfer*, **26(8)**, pp.1181-1188.
11. Hwang, D. H., Chang, S. H., 1994, Development of a phenomenological model for the prediction of dryout locations under flooding-limited critical heat flux conditions, *Nucl. Eng. Des.,* **148**, pp.475-486.
12. Tien, C. L., Chung, K. S., 1979, Entrainment limits in heat pipes, *AIAA J.*, **17**, pp.643-646.
13. Katto, Y., Hirao, T., 1991, Critical heat flux of counter-flow boiling in a uniformly heater vertical tube with a closed bottom, *Int. J. Heat Mass transfer*, **34(4/5)**, pp.993-1001.
14. Katto, Y., Watanabe, K., 1992, An analytical study on the critical heat flux of countercurrent boiling in a vertical tube with a closed bottom, *Int. J. Heat Mass Transf.*, **35**, pp.3021-3028.
15. Wallis, G. B., 1969, *One-dimensional Two-phase Flow*, McGraw-Hill, New York.

Table 1. Present test conditions and applicable ranges of the correlations of Park et al. (1997) and Chun et al. (2001)

	Present work	Park et al.	Chun et al.
Test section geometry	3 x 3 rod bundle	Round tubes, annuli and rectangular channels	Annulus
Fluid	Water	Water and Freon	Water
Hydraulic equivalent diameter (mm), (D_{hy})	8.81	4.8-17.2	9.86
Length to diameter ratio, (L_B/D_{he})	219.8-250.9	8.1-120.0	48.0-59.8
Liquid to vapor density ratio, (ρ_l/ρ_g)	6.2-348.4	200-1600	6.2-335.6
Bond number, (B_o)	4.5-8.6	1.79-17.3	4.25-10.0

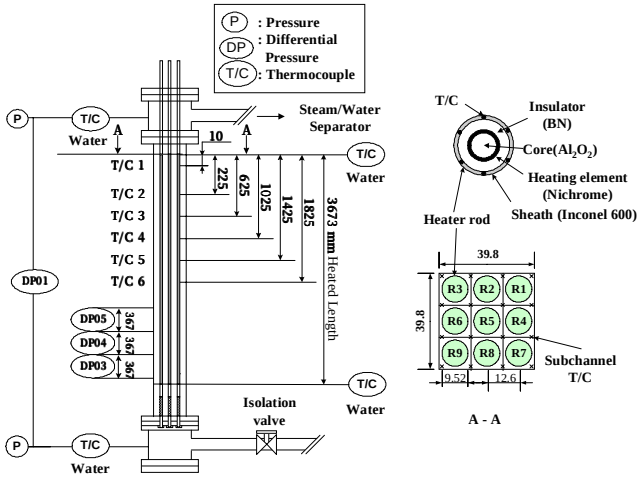

Fig. 1 Test section geometry and the locations of measuring sensors

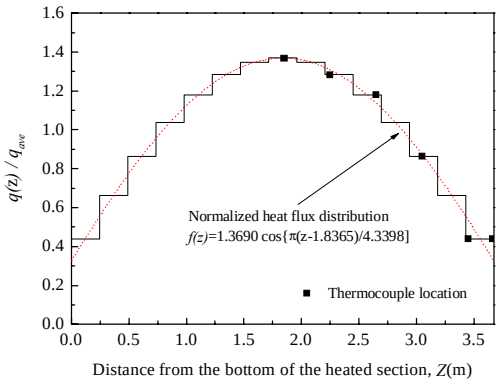

Fig. 2 Heat flux distribution

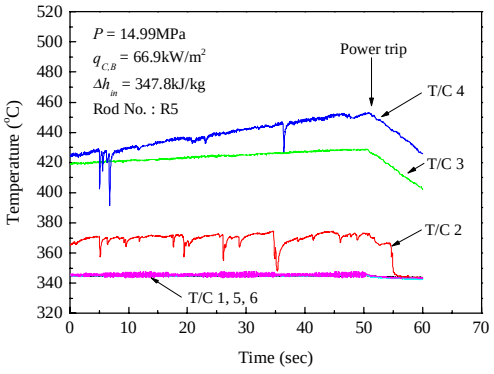

Fig. 3 Typical behavior of surface temperature of heater

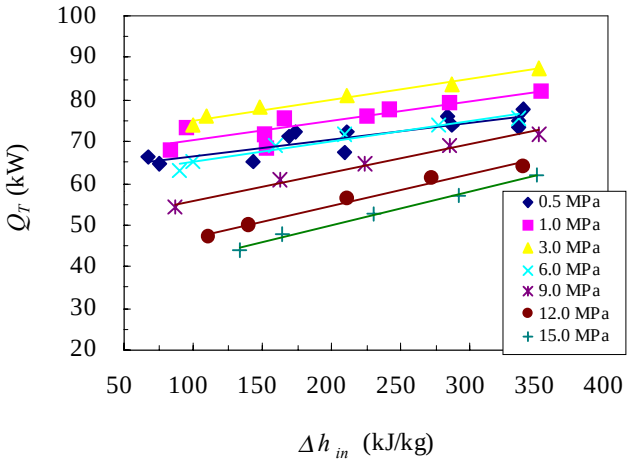

Fig. 4 The trend of the applied electrical power with the variation of the pressure and the inlet water subcooling enthalpy at the CHF condition

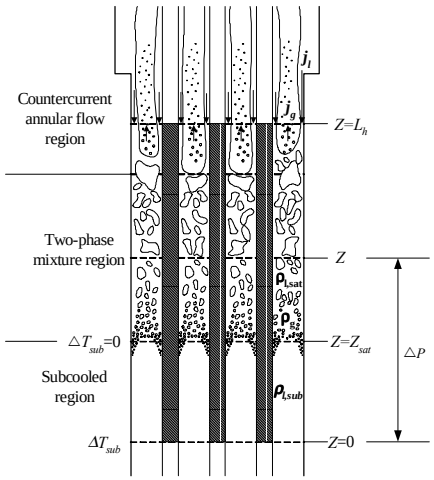

Fig. 5 Physical model of the present boiling system

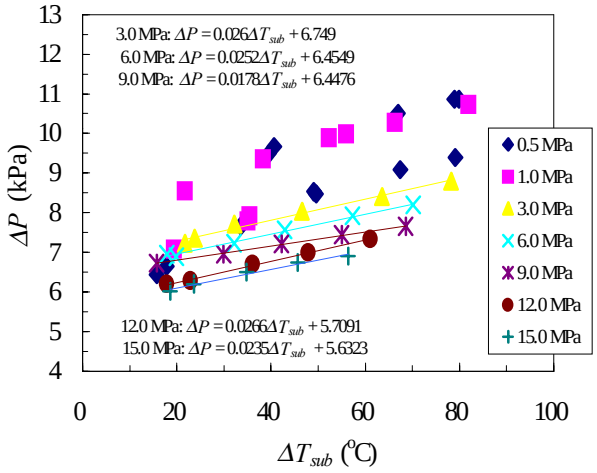

Fig. 6 Variation of pressure drop with subcooling temperature

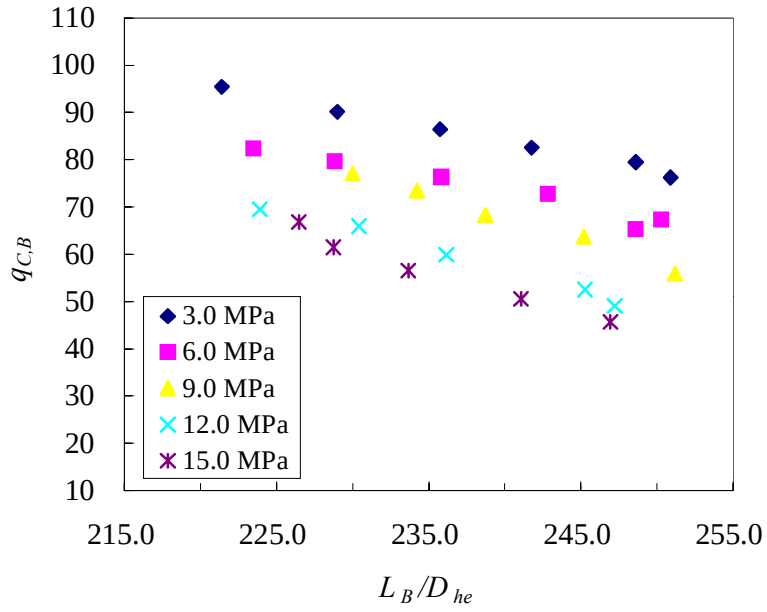

Fig. 7 Flooding CHF as a function of boiling length to heated equivalent diameter ratio

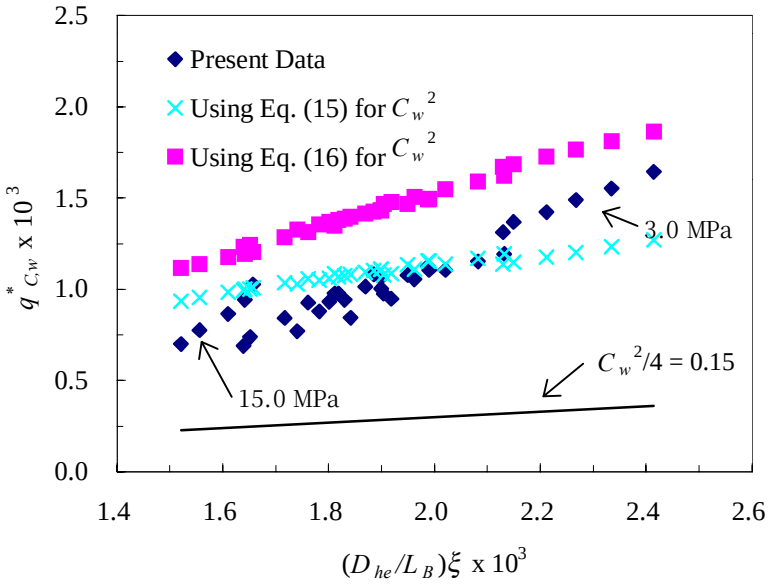

Fig. 8 Comparison of the present data with Eq. (10)

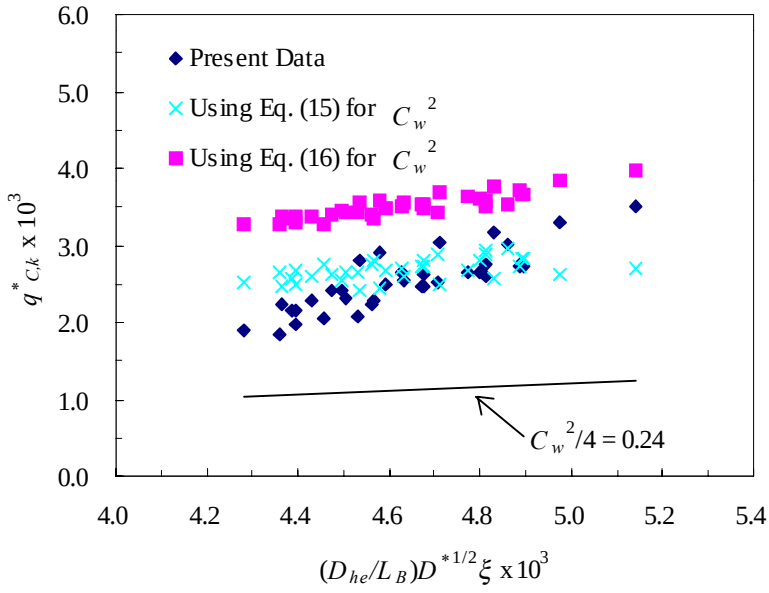

Fig. 9 Comparison of the present data with Mishima and Nishihara's equation (Eq(11))

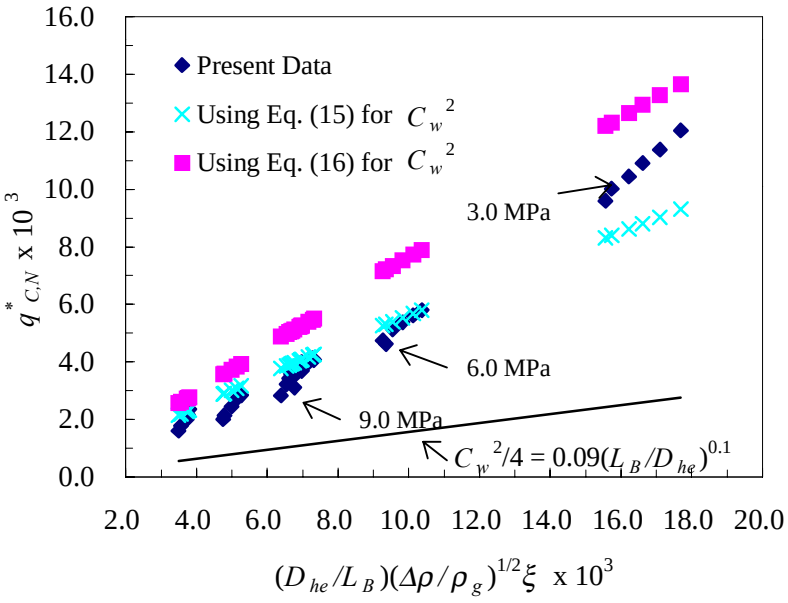

Fig. 10 Comparison of the present data with Nejat's equation (Eq(12))

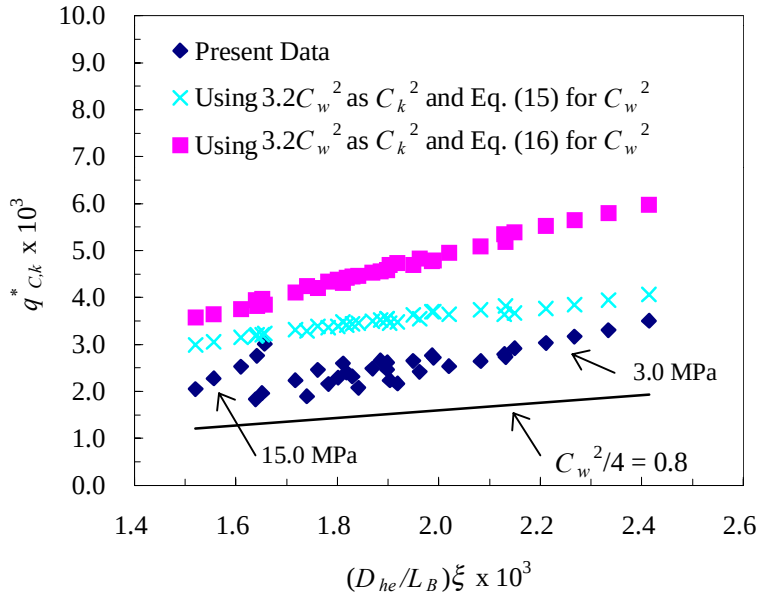

Fig. 11 Comparison of the present data with Tien and Chung's equation (Eq(13))

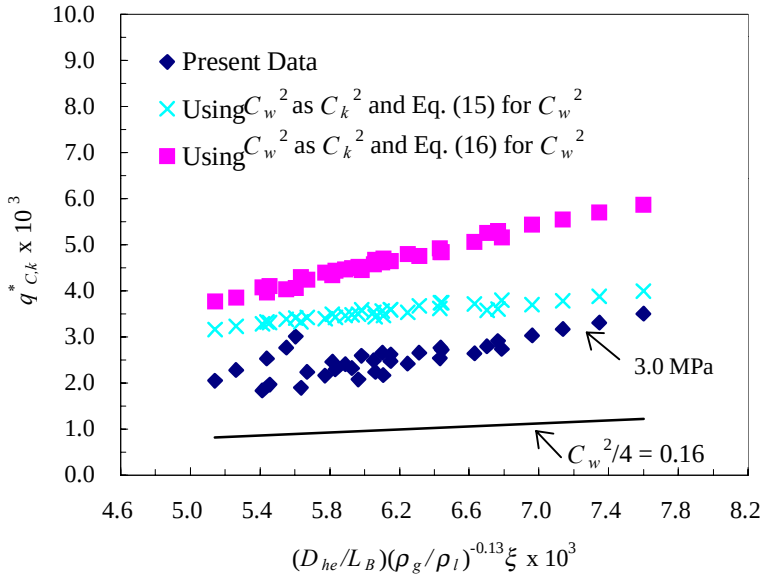

Fig. 12 Comparison of the present data with Imura et al.'s equation (Eq(14))